Graphene Plasmon Waveguiding and Hybridization in Individual and Paired Nanoribbons

Johan Christensen,[†] Alejandro Manjavacas,[†] Sukosin Thongrattanasiri,[†] Frank H. L. Koppens,[‡] and F. Javier García de Abajo[†,§,*]

[†]IQFR—CSIC, Serrano 119, 28006 Madrid, Spain and [‡]ICFO-Institut de Ciencies Fotoniques, Mediterranean Technology Park, 08860 Castelldefels, Barcelona, Spain. [§]Present address: Currently on sabbatical at Optoelectronics Research Centre, University of Southampton, Southampton SO17 1BJ, U.K.

ABSTRACT

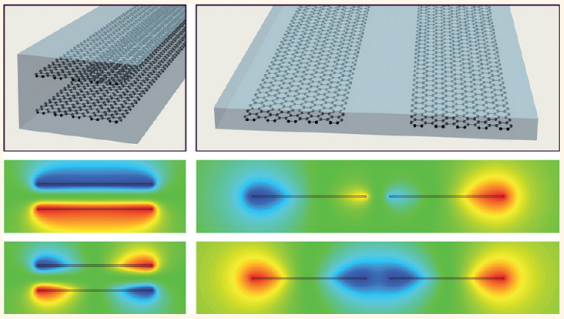

Plasmons in doped graphene exhibit relatively large confinement and long lifetime compared to noble-metal plasmons. Here, we study the propagation properties of plasmons guided along individual and interacting graphene nanoribbons. Besides their tunability *via* electrostatic gating, an additional handle to control these excitations is provided by the dielectric environment and the relative arrangement of the interacting waveguides. Plasmon interaction and hybridization in pairs of neighboring aligned ribbons are shown to be strong enough to produce dramatic modifications in the plasmon field profiles. We introduce a universal scaling law that considerably simplifies the analysis an understanding of these plasmons. Our work provides the building blocks to construct graphene plasmon circuits for future compact plasmon devices with potential application to optical signal processing, infrared sensing, and quantum information technology.

KEYWORDS: plasmonics · graphene plasmons · nanophotonics · waveguides · nanoribbons

Plasmons, the collective oscillations of conduction electrons, have been identified in a large variety of systems, ranging from metallic films[1] down to nanoparticles[2] and carbon molecules,[3] and more recently also in graphene.[4] In an intuitive picture to understand these excitations, the electric field of an incident light beam can drive a collective spring motion of free charges (the conduction electrons) back and forth between opposite ends of a metal structure.[2] The importance of such motion lies in part in its ability to focus light and enhance the electric field intensity near the structure by several orders of magnitude, which allows sensing chemical changes in the immediate vicinity of the particle,[5] as well as performing surface-enhanced Raman scattering (SERS) down to the single molecule level.[6] Field enhancement is particularly intense in metallic gaps, which can now be reliably fabricated below 10 nm.[7] New plasmonic nanostructures with added functionalities are currently emerging at a tremendous pace.[8−10] In this context, plasmon hybridization has emerged as a popular approach to understand and predict the properties of these excitations by relying on the methods of quantum chemistry,[11,12] which allow tuning nanometer-sized particles to the desired wavelength region, leading to applications such as cancer therapy.[13,14]

The relatively short lifetime of confined plasmons, typically in the range of tens of optical cycles, is a limiting factor for many potential applications. Additionally, plasmons are difficult to control without producing changes in the composition or geometry of the nanostructures on which they are supported. These limitations have been recently lifted with the recent prediction[15−18] and indirect observation[4] of plasmons in doped graphene, which are expected to live much longer[18] and can be controlled by varying the doping level *via* electrostatic gating.[19]

The unique electronic, mechanical, and optical properties of graphene[20−27] have spurred tremendous interest on this atomically thin material, from which applications such as optical sensors,[28] transparent electrodes, and NEMs[23] are rapidly emerging. The linear dispersion relation of electronic states in graphene, characterized by conical conduction and valence bands joined by just two single points at the Fermi

* Address correspondence to J.G.deAbajo@csic.es.

Received for review October 2, 2011 and accepted November 25, 2011.

Published online December 06, 2011
10.1021/nn2037626

level (the so-called Dirac points),[25,29] makes it a fantastic material for optoelectronic applications.[19,24,27,28,30−32] Additionally, an excess of electrons or holes in doped graphene can produce collective plasmon oscillations, similar to those in noble metals.[15−18] However, compared to conventional plasmonic materials (*e.g.*, silver and gold), graphene with elevated carrier densities presents the following appealing properties:[33]

- *Tunability*. The optical response of doped graphene strongly depends on the doping level, or equivalently, on the Fermi energy E_F relative to the Dirac points, which can be chemically or electrostatically tuned, thus resulting in dramatic changes in the plasmon spectrum. This actually provides a tool for electrically switching the optical properties of the carbon sheet.[19] Fermi energies of the order of an electronvolt are currently attainable,[34,35] involving charge-carrier densities $n = E_F^2/(\pi\hbar^2 v_F^2) \approx 10^{14}$ cm^{-2}, where $v_F \approx c/300$ is the Fermi velocity.
- *Extreme confinement*. Doped-graphene plasmons have a wavelength λ_p that is *ca.* 1−3 orders of magnitude smaller than the light wavelength λ_0 (more precisely, $\lambda_p/\lambda_0 \approx 2\alpha E_F/(\hbar\omega)$, where $\alpha \approx 1/137$ is the fine structure constant and ω is the light frequency). This is because these plasmons propagate at a speed comparable to $v_F \ll c$. As a result, graphene plasmons can be confined down to volumes that are several orders of magnitude smaller than plasmons in noble metals.
- *Crystalinity*. The strength of the carbon chemical bond produces regular graphene structures that are defect-free over several plasmon wavelengths.[36] This is in contrast to metal plasmonics, in which fabrication imperfections constitute a bottleneck in the performance of nanometallic structures.
- *Low losses*. The relatively large conductivity of graphene translates into long optical relaxation times reaching values of $\tau \approx 10^{-13}$ s, compared to $\sim 10^{-14}$ s in gold, thus providing a plausible solution to the long-standing problem of dissipation in plasmonics. The lifetime of graphene plasmons can reach hundreds of optical cycles and, at higher frequencies and carrier densities, it is only limited by the intrinsic relaxation time of this material. For energies above 0.2 eV, graphene optical phonons are expected to dominate plasmonic losses, but careful analysis[37] reveals that the effective scattering time can still be larger than for noble metals. We remark that low losses are only expected for sufficiently high carrier densities, such that the Fermi energy is larger than the plasmon energy.[33]

Because of these unique properties, graphene has been recently proposed as a platform for plasmon waveguiding at infrared frequencies, in particular by patterning a back gate to draw plasmon circuits and optical elements in the doped regions of an extended graphene sheet placed above the patterned gate.[38] A surface cloak based on graphene has been recently proposed as well.[39] Plasmons in suitably nanostructured graphene have been shown to produce strong cavity-QED effects[33] and total infrared light absorption.[40] Even unpatterned graphene can lead to a tremendous reduction in the lifetime of neighboring excited atoms by up to 5−6 orders of magnitide due to plasmon coupling.[33,41−43] From the experimental side, graphene plasmons are being intensely investigated, and even metamaterials integrating graphene have been recently produced.[4,44] Clear evidence of the effect of graphene plasmons in the THz transmission properties of microribbons has been recently obtained, conclusively demonstrating the ability to control the optical properties of this material by electrostatic doping.[4]

In this work, we show that doped graphene ribbons can propagate plasmons along large distances compared to the plasmon wavelength. Waveguides are a central element for plasmonic applications, and in particular, graphene waveguides inherit all of the advantages noted above and present unique features, such as a large concentration of the electromagnetic field near ribbon edges and strong interaction that can be useful to transfer information between neighboring waveguides. In combination with other appealing graphene properties, such as its high electron mobility, this opens new avenues for optoelectronic applications, sensors, and quantum information transfer. We supplement this study by formulating a powerful universal scaling law that allows one to apply our results to any geometrically scaled structure without requiring further extensive numerical computations.

It should be noted that our study is based upon a classical electromagnetic description in which graphene is represented by a local conductivity. We have shown that this is accurate for ribbons wider than 25 nm, such as those considered here, compared to an *ab initio* theoretical description of the optical response of these structures.[45]

RESULTS AND DISCUSSION

Individual Ribbons. We start by analyzing individual ribbons in Figure 1. The translational symmetry of the system permits classifying all electromagnetic solutions (including propagating plasmons) in terms of their frequency ω and parallel wave vector $k_{||}$, so that the corresponding fields and induced currents depend on time t and distance z along the ribbon as exp $(ik_{||}z - i\omega t)$. In the dispersion diagram of Figure 1a, calculated for a ribbon width $W = 100$ nm, the light line is nearly indistinguishable from the vertical axis

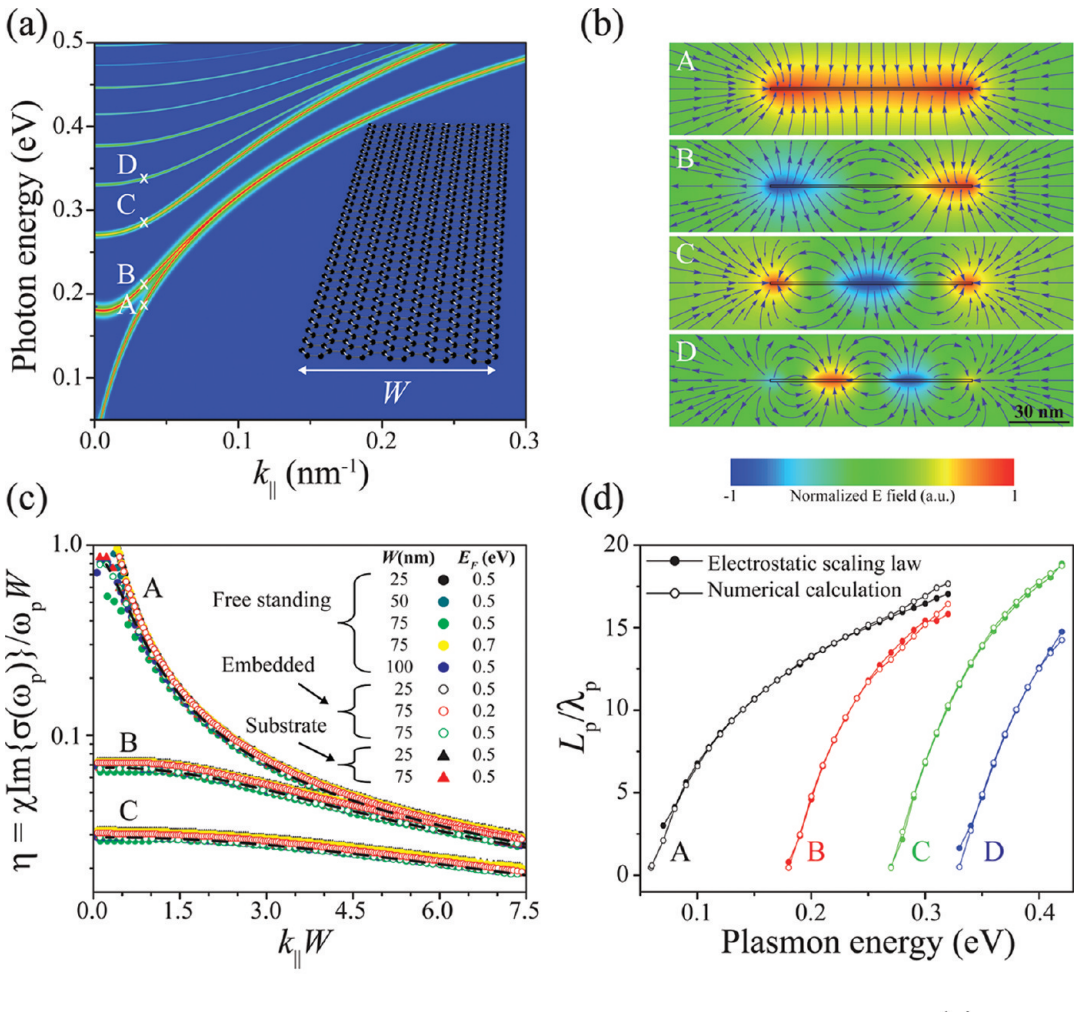

Figure 1. Guided plasmons in individual doped graphene ribbons. (a) Dispersion diagram of a self-standing ribbon of width $W = 100$ nm and Fermi energy $E_F = 0.5$ eV. (b) Real part of the electric field amplitude (density plots) along the ribbon direction corresponding to modes labeled A−D in panel (a) for a parallel wave vector $k_{\parallel} = 0.035$ nm^{-1} and energies 0.19, 0.22, 0.29, and 0.34 eV, respectively. The field lines for the electric field components in the plane of the figure are shown by arrows. (c) Universal electrostatic scaling parameter $\eta = \chi\ \mathrm{Im}\{\sigma(\omega_p)\}/(\omega_p W)$, where ω_p refers to the plasmon peak frequencies, as a function of $k_{\parallel} W$ for ribbons with different values of W and E_F in various dielectric environments: free-standing ($\chi = 1$), embedded in silica ($\chi = 1/\varepsilon_s$ with $\varepsilon_s = 2.1$), and supported on a substrate−air interface ($\chi = 2/(\varepsilon_s + 1)$). (d) Propagation distance in units of the plasmon wavelength for modes A−D as obtained from the electrostatic scaling law (solid symbols) and from the width of the plasmon features in panel (a) (open symbols).

(*cf.* the horizontal scale of the figure and the light wave vector $k_{\parallel} = 0.0025$ nm^{-1} at $\hbar\omega = 0.5$ eV), so the plasmon bands under consideration are essentially electrostatic in nature, which is actually expected from the small ribbon width compared to the photon wavelength (*e.g.*, even at 0.5 eV, the photon wavelength is 25 times larger than the ribbon width in Figure 1a). The quantity actually plotted in Figure 1a is the local density of optical states (LDOS, see Materials and Methods), which show prominent maxima at points ($k_{\parallel}$,ω) corresponding to the presence of graphene plasmons. The lowest-energy mode A displays a characteristic wavelength-cutoff-free profile typical of any linear trapping structure (*e.g.*, nanowires, dielectric fibers, *etc.*), and asymptotically approaching the light line in the $k_{\parallel} W \rightarrow 0$ limit. The electric near-field along the ribbon direction (Figure 1b) demonstrates that this mode is a 2D monopole, characterized by the absence of any nodes in the induced density across the ribbon width (notice that the field lines of the field components in the plane of the figure, indicated by arrowed lines in Figure 1b, are nearly perpendicular to the ribbon close to it, where the normal field at the ribbon is proportional to the induced surface charge density, which indeed does not change sign in mode A). This so-called edge mode[46] has maxima of intensity near the ribbon boundaries. In contrast to mode A, higher-energy modes (*e.g.*, B−D in Figure 1a) display a characteristic optical dispersion, with a threshold energy toward $k_{\parallel} = 0$ at which their group velocity vanishes. These modes have been extensively studied for $k_{\parallel} = 0$,[33] where they have been shown to couple to propagating light as dipoles and higher order multipoles depending on the number of nodes because their wave vector lies

inside the light cone, although their main source of attenuation is absorption losses in the carbon sheet (*e.g.*, coupling to electron−hole pairs and phonons), rather than radiation.[33] Actually, all modes, including A, have a similar fwhm, approximately equal to $\hbar\tau^{-1}$ (see below).

The near-field plots of Figure 1b show that modes A−D are 2D monopoles, dipoles, quadrupoles, and octopoles, respectively. Strong field concentration takes place at the ribbon edges in all cases. These characteristics are maintained all along the dispersion curves.

Electrostatic Scaling Law. The electrostatic nature of the modes suggests that we can formulate a simple scaling law allowing us to obtain universal plasmon dispersion curves, with independence of the ribbon width, the actual model used for the conductivity σ, and the physical parameters of the graphene (*i.e.*, E_F, τ, and the temperature). A scaling law has already been hinted within the Drude model,[4] but we here present a general formulation that is applicable to any form of σ and extends not only to the plasmon frequencies but also to their lifetimes. Unlike electrodynamics, in which the wavelength defines an absolute length scale, the electrostatic limit is scale-invariant. The plasmon resonances of the system are thus solely determined by the geometry and the dielectric function. Examining the dielectric function used in our simulations of graphene ribbons (see Materials and Methods), and noticing that our results have reasonably converged for the small thickness under consideration (see Supporting Information, SI), we conclude that the plasmon energies must occur at specific values of the dimensionless parameter $-i\sigma(\omega)/(\omega W)$ (we use Gaussian units here, so σ has dimensions of velocity). Neglecting losses, we conclude that the values of the scaling parameter

$$\eta = \chi\frac{\mathrm{Im}\{\sigma(\omega_p)\}}{\omega_p W} \qquad (1)$$

at the peak plasmon frequencies ω_p must be independent of W, E_F, and other physical parameters, and therefore, η is only a function of the product $k_{||}W$. (We introduce the factor $\chi = 1$ in vacuum, and $\chi \neq 1$ near dielectrics; see below). We illustrate this in Figure 1c, which shows the scaling parameter corresponding to plasmons calculated for a wide range of values of W and E_F. The scaling law is remarkably fulfilled, thus simplifying the task of dealing with different ribbon widths and doping levels, as the plasmon energies can be constructed by finding the values of ω_p that follow the universal curves presented in Figure 1c. Incidentally, we show in the SI several of the dispersion diagrams from which Figure 1c has been extracted, corresponding to a wide range of graphene physical parameters. The black dashed curves are analytical fits to the data given by

$$\eta = -0.0023 + 0.25/(2.7 + k_{||}W) + 0.28/(0.34 + k_{||}^2W^2) \quad \text{mode A}$$
$$\eta = 0.0107 + 1.05/[18.5 + (k_{||}W - 0.307)^2] \quad \text{mode B}$$
$$\eta = 0.00519 + 1.56/[65.7 + (k_{||}W - 0.211)^2] \quad \text{mode C}$$

These expressions in combination with eq 1 provide a comprehensive description of the guided mode energies in graphene ribbons.

It is instructive to insert the Drude model (see Materials and Methods) in eq 1 to obtain an analytical expression for the plasmon frequencies,

$$\omega_p = \frac{e}{\hbar}\sqrt{\frac{\chi E_F}{\pi\eta W}} \qquad (2)$$

Similar to plasmons in a homogeneous graphene sheet,[18] eq 2 predicts a plasmon frequency scaling with $(E_F)^{1/2}$. For fixed $k_{||}W$ (this implies fixed η), the frequency scales like $1/\sqrt{W}$, in agreement with previous observations for $k_{||} = 0$.[4,33] Naturally, the plasmon frequency can be influenced by finer details in the conductivity σ beyond the dipole model, but the universal scaling law of eq 1 can be applied for any form of the frequency-dependent function $\sigma(\omega)$. Interestingly, guided modes do not satisfy the typical thumb rule of classical waveguides in which the first mode occurs for a width given by $\lambda_p/2$. Instead, the ribbon width for which a mode can be guided is related to the plasmon wavelength in homogeneous graphene through a less intuitive relation,

$$W = \frac{\lambda_p}{4\pi^2\eta} \qquad (3)$$

where η can be directly plugged from Figure 1c as a function of $k_{||}W$ for low-energy guided modes. Equation 3 is obtained by expressing eq 1 (with $\chi = 1$ for self-standing ribbons) in terms of the plasmon wavelength, $\lambda_p = 4\pi^2\,\mathrm{Im}\{\sigma(\omega_p)\}/\omega_p$, which is in turn derived from the plasmon dispersion relation in homogeneous graphene $k_{||}^{SP} = i\omega/[2\pi\sigma(\omega)]$.[18] Incidentally, the dispersion relation of the wavelength-cutoff-free mode (A in Figure 1) asymptotically converges to the latter expression in the $k_{||}W \ll 1$ limit.

We provide two modifications of the scaling law intended to deal with relevant configurations in which the graphene is placed near dielectrics: (1) when the carbon sheet is fully embedded in a homogeneous medium of permittivity ε_s, the fields produced by the charges induced in the graphene are effectively reduced by a factor $\chi = 1/\varepsilon_s$, and thus, the above scaling law works if we multiply the scaling parameter by this coefficient; (2) likewise, the electrostatic field produced by charges sitting on a planar interface of this dielectric with air are simply reduced by a factor $\chi = 2/(\varepsilon_s + 1)$, which therefore needs to be multiplied to the scaling parameter when describing supported graphene. The scaling law is also shown in Figure 1c to apply to these two additional configurations (homogeneous dielectric and dielectric substrate).

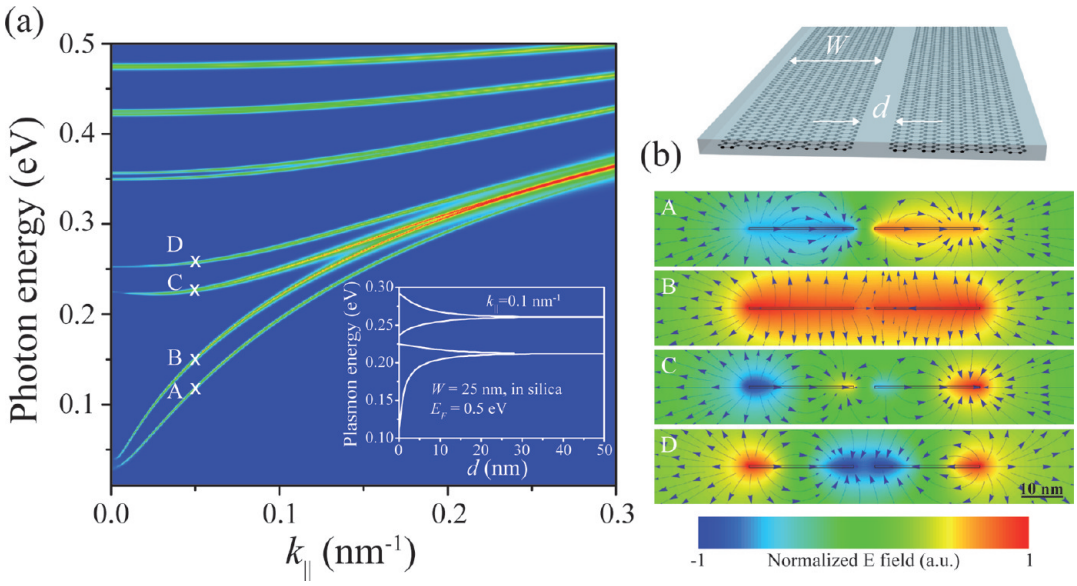

Figure 2. Hybridized plasmons in aligned ribbon pairs: coplanar configuration. (a) Dispersion diagram for two ribbons of width W = 25 nm and Fermi energy E_F = 0.5 eV embedded in silica and separated a distance d = 5 nm. The inset shows the d dependence of the plasmon energy in the four lowest-energy modes (labeled A−D in the main plot) for fixed parallel wave vector $k_{||}$ = 0.1 nm^{-1}. (b) Electric near-field (using the convention of Figure 1) of modes A−D in panel (a) at energies of 0.12, 0.15, 0.23, and 0.27 eV, respectively, and a common value of $k_{||}$ = 0.05 nm^{-1}.

When losses are contemplated, the scaling parameter must remain real at the plasmon resonance (that is, in contrast to electrodynamics, electrostatics can be constructed out of real quantities because there are no radiative losses involved). This reality condition allows us to estimate the frequency fwhm of the modes, which is given by the on-resonance value of $-2\mathrm{Im}\{\omega_p\}$. Actually, the frequency enters the graphene permittivity roughly *via* $\omega(\omega + i\tau^{-1})$, which takes a real value when $\mathrm{Im}\{\omega\} = (-1/2)\tau^{-1}$, for which σ becomes purely imaginary. The frequency fwhm of the modes must therefore be equal to τ^{-1}, and their lifetime is thus independent of ribbon width and parallel wave vector.

The scaling law obviously applies to any geometry by substituting a characteristic length of the structure for W. In particular, the computations that follow for ribbon pairs can be applied to any other structure in which the ratio of ribbon distance to width is kept constant.

Propagation Distance. The distance traveled by plasmons before they are dissipated into electron−hole pairs and heat is essentially controlled by their lifetime. We have shown from the electrostatic scaling law that the lifetime is basically the same as the *bulk* relaxation time of graphene τ, and therefore, the propagation distance is simply given by $v_g\tau$, where v_g is the group velocity (*i.e.*, the slope of the dispersion curves, $v_g = d\omega_p/dk_{||}$). Expressed in units of the plasmon wavelength $\lambda_p = 2\pi/k_{||}$, a plasmon of wave vector $k_{||}$ travels a distance

$$\frac{L_p}{\lambda_p} = \frac{k_{||} v_g \tau}{2\pi} \qquad (4)$$

before it is dissipated. We show in Figure 1d propagation distances derived from this expression for modes A−D of 1a (solid symbols), in agreement with recently reported calculations.[46] This agreement is expected because the electrostatic limit is a good approximation to study ribbons of small width compared to the wavelength. Equation 4 clearly explains the observed vanishing of L_p/λ_p in the limit of small $k_{||}$. Interestingly, the distance L_p reaches many plasmon wavelengths, a behavior that is not found in thin noble-metal waveguides for similar small values of λ_p.

These results are in excellent agreement with a direct calculation of the propagation distance obtained from the width of the plasmon features in Figure 1a. More precisely, the wave-vector dependence of the LDOS shown in this figure near a plasmon resonance at fixed frequency is simply given by a Lorentzian, $\sim 1/[(k_{||} - Re\{k_{||}^{SP}\})^2 + (\mathrm{Im}\{k_{||}^{SP}\})^2]$, where $k_{||}^{SP}$ is the complex plasmon wave vector, the imaginary part of which describes 1/*e*—intensity attenuation along the direction of propagation with a characteristic distance

$$L_p = 1/(2\mathrm{Im}\{k_{||}^{SP}\}) \qquad (5)$$

(open symbols in Figure 1d). Here, $2Im\{k_{||}^{SP}\}$ is directly extracted from the fwhm of the plasmon feature along $k_{||}$ for fixed frequency.[47] The agreement between the results of eq 4 and eq 5 further corroborates the validity of the electrostatic scaling law, thus providing a simple recipe to estimate the propagation distance from the dispersion curves for any ribbon size using eq 1 and eq 4. This is a useful general result that can be applied to any graphene geometry, including the ribbon pairs studied below, in which one only needs to find the optical response for a given size of the system, from which the response of a

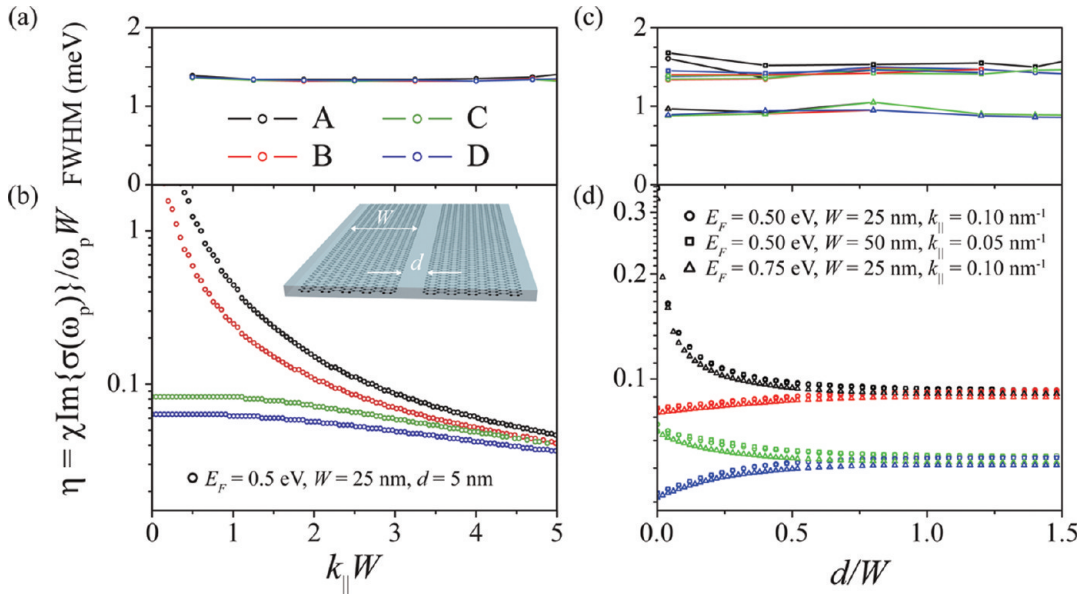

Figure 3. Electrostatic scaling in coplanar ribbon pairs. (a,b) Plasmon fwhm (a) and scaling parameter η (b) as a function of normalized parallel wave vector $k_{||}$ for the same ribbon pairs and modes A−D as in Figure 2. (c,d) Plasmon fwhm and scaling parameter as a function of ribbon separation d normalized to the ribbon width W for three different combinations of Fermi energy E_F and W. Notice that $k_{||}$ is varied in (c,d) in order to maintain $k_{||}W$ constant in all three calculations.

geometrically scaled structure follows using the above expressions.

Coplanar Ribbon Pairs. The interaction between guided plasmons in a pair of coplanar aligned ribbons embedded in homogeneous silica is analyzed in Figure 2. Each of the individual ribbon modes is observed to split into two hybridized modes (Figure 2a). This splitting is obviously increasing with decreasing separation d, as shown in the inset of Figure 2a for the four lowest-energy modes labeled A−D in the main plot. The lowest energy mode goes to zero energy at $d = 0$, whereas the other three modes approach a finite limiting energy. This behavior is further explained by the near-field plots of Figure 2b, in which the two lowest-energy modes (A and B) are seen to originate in the hybridization of the fundamental monopolar modes of the individual ribbons (*i.e.*, similar to mode A of Figure 1); in particular, the lowest-energy mode (A) is a binding state, in which the monopoles have opposite charges, and in the limit of small separations it migrates toward the red, eventually disappearing as a frozen mode. However, the second mode (B) involves monopoles of equal charge, and in the limit of touching ribbons it smoothly converges to the monopole of the ribbon of double width; this is a smooth transition between the touching and nontouching regimes, unlike what happens in sphere dimers.[48] The third and fourth modes (C and D) are binding and antibinding hybridizations of the dipole modes of the individual ribbons (*i.e.*, similar to mode B of Figure 1), which combine to form the dipole mode (C) and the quadrupole mode (D) of the ribbon of double width in the touching limit. As a thumb rule, the interaction between plasmons in coplanar ribbon pairs gives rise to hybridized states, with small splitting at large separations, and converging to the modes of the ribbon of double width at zero separation; hybridization of modes of order $n = 0, 1, \ldots$ (monopoles, dipoles, *etc.*) smoothly gives rise to double-width-ribbon modes of orders $2n$ and $2n - 1$ in the touching limit, except the monopoles ($n = 0$), which only produce a double-width monopole when touching, as the lowest-energy hybridized mode goes to zero frequency and disappears at vanishing separation. This story is further supported by dispersion diagrams for larger separations, and it also applies to ribbons supported on a dielectric surface, with just quantitative modifications due to the factor χ discussed above (see SI).

Like in individual ribbons, the near-field plots of Figure 2 show that ribbon edges concentrate electromagnetic energy. This is specially emphazied by the hybridized dipole modes C and D in Figure 2b.

The validity of electrostatic scaling in ribbon pairs is illustrated by Figure 3. The scaling parameter $\eta = \chi \mathrm{Im}\{\sigma(\omega_p)\}/(\omega_p W)$ obtained from the dispersion curves A−D of Figure 2a is shown in Figure 3b, and the corresponding plasmon widths are represented in Figure 3a. Notice that Figure 2 is calculated for ribbons embedded in silica, and therefore, we have used $\chi = 1/\varepsilon_s$ in the above formula in order to compensate for the effect of the dielectric. As expected, the fwhm shows a rather flat profile, roughly concentrated near the intrinsic width $\hbar\tau^{-1} \approx 1.32$ meV. Clearly, η should only depend on the ratio d/W and the product $k_{||}W$. Here, we only present a limited range of calculations, which can then be extrapolated to ribbons of different width W. In particular,

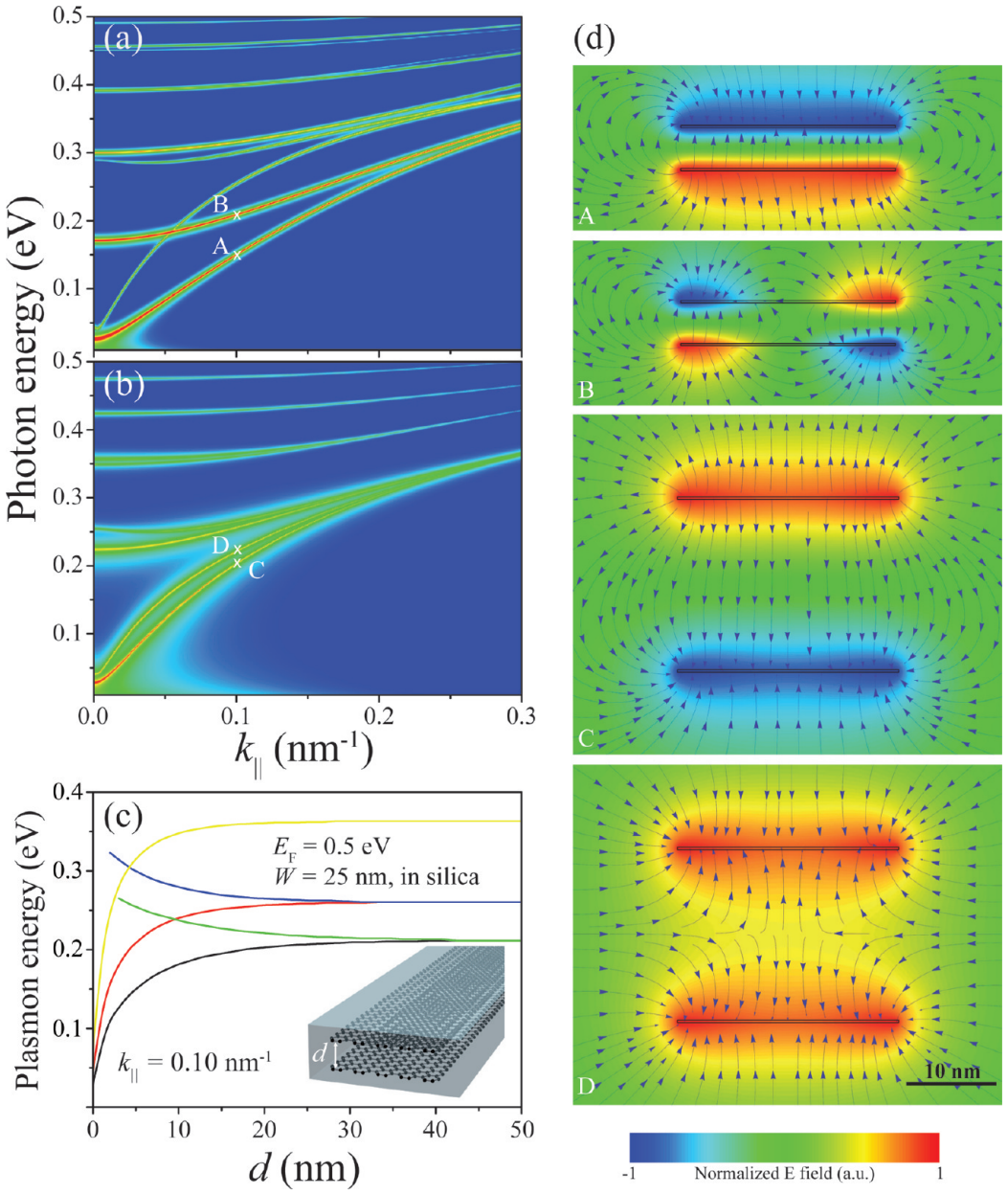

Figure 4. Hybridized plasmons in aligned ribbon pairs: vertically offset configuration. (a,b) Dispersion diagram for two ribbons of width W = 25 nm and Fermi energy E_F = 0.5 eV embedded in silica and separated by a distance d = 5 nm in panel (a) and d = 20 nm in panel (b). (c) Plasmon energy dependence of the five lowest-energy modes as a function of d for fixed parallel wave vector $k_{||}$ = 0.1 nm^{-1}. (d) Electric near-field (using the convention of Figure 1) of modes labeled A–D in panels (a–c), corresponding to $k_{||}$ = 0.1 nm^{-1}; d = 5 nm in A and B; d = 20 nm in C and D; and energies of 0.15 (A), 0.21 (B), 0.20 (C), and 0.22 eV (D).

Figure 3c,d shows the ribbon-distance dependence of the scaling parameter calculated for various combinations of Fermi energy and ribbon width, with $k_{||}$ also varied to keep $k_{||}W$ fixed. These combinations lead to very close values of η for the four lowest-energy plasmons under consideration (Figure 3d). In contrast, the fwhm of these modes (Figure 3c) is peaked around two different values, roughly given by $\hbar\tau^{-1} \approx 1.32$ meV for E_F = 0.5 eV and $\hbar\tau^{-1} \approx 0.88$ meV for E_F = 0.75 eV. Finally, in the $d/W \gg 1$ limit we recover the two lowest-energy modes of individual ribbons for $k_{||}W$ = 2.5 (see Figure 1c).

Vertically Offset Ribbon Pairs. Plasmon hybridization in vertically offset ribbons is quite different from coplanar ribbons, as shown in Figure 4. At large separations, weak mode hybridization and splitting occurs, preferentially involving pairs of initially degenerate states (one per ribbon). For example, two monopole modes (like mode A in Figure 1) are combined to form two hybridized states, giving rise to the two lowest-energy bands of Figure 4b. The near fields of these modes basically show binding and antibinding combinations of monopoles, without nodes in the induced charge of each ribbon (Figure 4d, modes C and D, respectively). In

contrast, the lowest-energy modes at smaller separations (A and B in Figure 4d) have very different origin, as A is still an antisymmetric combination of monopoles, whereas B is an antisymmetric combination of dipoles. The transition between these two regimes as the distance d is decreased is clearly observed in Figure 4c, in which nonavoided crossings are taking place, and in particular the second mode converges to the fundamental one for large d because both of them are monopole−monopole combinations, whereas it is replaced by the dipole−dipole binding state below $d \approx 10$ nm. This effect is also observed in the dispersion diagram of Figure 4a as a mode crossing between the second and third modes at low values of $k_{||}$. These are nonavoided crossings because they involve noninteracting modes of different symmetry.

CONCLUSIONS

We have presented a comprehensive analysis of guided plasmons in individual and paired graphene ribbons, thus providing one of the central elements needed to construct plasmon circuits in graphene at infrared frequencies. Our critical findings are as follows: (1) Individual ribbons are shown to exhibit a band structure similar to narrow dielectric waveguides and plasmonic nanowires,[47] characterized by a fundamental acoustic mode (*i.e.*, a band without a wavelength cutoff) and a discrete set of higher-energy optical modes (converging to nonpropagating plasmons that couple to radiation[33] for $k_{||} < \omega/c$); (2) unlike thicker plasmonic waveguides in noble metals,[49,50] plasmons propagating in graphene ribbons exhibit a large concentration of the electric field near the edges, particularly in ribbon pairs placed at close proximity; (3) the plasmon dispersion relation can be engineered by changing the distance and relative configuration of the ribbons in a pair; (4) we have formulated an electrostatic scaling law (see eq 1) that facilitates the understanding of these plasmons by allowing us to obtain their wavelengths and propagation distances from universal curves exclusively as a function of $k_{||}W$ and the aspect ratio in the ribbon pairs (d/W). In brief, ribbons provide a convenient way to guide plasmons, with highly customizable dispersion bands. We have also explored plasmon hopping between graphene disks as an alternative guiding configuration, but the strong trapping of plasmons in these structures averts the possibility of having a reasonably intense interaction between neighboring disks, and consequently the resulting dispersion bands are rather flat (see SI). Our results are based upon classical electromagnetic theory, in which the graphene is described by a frequency-dependent conductivity σ, but careful analysis of nonlocal effects (*e.g.*, band gap opening[51] and edge electron scattering and binding[25,52]) must be made before extrapolating these conclusions to small widths below a few tens of nanometers.

The electrostatic tunability and relatively long propagation distances of graphene compared to conventional plasmonic metals are excellent handles to design devices in which the plasmon wavelength, the propagation distance, and the dispersion characteristics of the ribbon waveguides are modified at will simply by applying an external potential.[4] In this respect, it should be noted that the propagation distance expressed in terms of the plasmon wavelength is directly proportional to the relaxation time τ (see eq 5), and therefore, τ is a critical parameter on which the range of applications of graphene plasmonic waveguides is pending. Although impurities, phonons,[18] and many-body effects[53] can drastically reduce the relaxation time, the estimated values based upon the measured electron mobility[20,54] are still well below the level of losses in conventional plasmonic metals for such degree of confinement ($\lambda_p \ll$ light wavelength). In this respect, plasmon lasing assisted by a surrounding gain material can be useful to extend plasmon lifetimes and propagation distances.[55]

Field enhancement at ribbon edges, particularly in ribbon pairs, can be advantageous to sense low-energy electronic and vibrational excitations of molecules sitting in their vicinity. Additionally, graphene waveguides provide a suitable way to extract any molecule-specific optical signal (*e.g.*, SERS and SEIRA) through guided modes, which can be subsequently processed (*e.g.*, they can be energy filtered by patterned graphene waveguides and resonant cavities) and detected (*e.g.*, by direct electron−hole separation). Incidentally, these guided plasmons can be created by sending external light to a decorated part of the ribbon (*e.g.*, *via* a nanoparticle) in order to access modes of large $k_{||}$ outside the light cone.

In a different application, the vertically offset configuration of Figure 4 can be used to couple the mechanical modes of a suspended graphene ribbon and the plasmons of the ribbon pair formed together with a second ribbon situated underneath. Although more technically challenging, the coplanar configuration of Figure 2 can serve this purpose by patterning a gap in the center of a wider suspended ribbon, so that mechanical vibrations would involve lateral and vertical displacements that periodically change the gap distance. Small variations in the distance between ribbons have been shown to produce large modifications in the plasmon dispersion relation, so that a guided plasmon signal of fixed frequency can only be on resonance at a specific separation, and therefore, a plasmon of appropriate frequency can produce attraction or repulsion between neighboring ribbons and as a result it can either stimulate or cool mechanical motion in these systems. This can be used in combination with plasmon pulses created by coupling to external light and acting during the larger between the pulse duration and the lifetime of the plasmon

(subpicoseconds). The latter is much shorter than the period of typical mechanical oscillations (well above the nanosecond), and therefore, plasmon pulses can act as sharp, synchronized impulses to classically control the spring motion with either attractive or repulsive forces depending on the symmetry of the modes (*e.g.*, mode D of Figure 4 should produce a repulsive force, because it involves charges of the same sign in both ribbons, in contrast to modes A–C). Finally, graphene ribbon waveguides, in combination with resonant graphene cavities operating at the single-plasmon level,[33] are potential candidates for a future quantum technology based on graphene plasmons and working under ambient conditions.

MATERIALS AND METHODS

We study guided plasmons in individual ribbons and ribbon pairs by examining the local density of optical states (LDOS), which we resolve in wave vectors $k_{\|}$ along the direction of ribbon translational invariance. The LDOS stands for the sum of normalized electromagnetic-mode intensities at a given spatial position[56] as a function of light frequency, so that it exhibits spectral peaks signaling the presence of localized modes, such as plasmons. Specifically, we compute the LDOS near the edge of the ribbons under consideration, where most modes make substantial contributions. We rigorously solve the Maxwell equations by means of the boundary element method (BEM)[57] to obtain the LDOS, as well as near fields of the modes (these fields are extracted from the induced electric field upon excitation by a nearby external dipole source). In this electromagnetic description, graphene is modeled as a thin layer of thickness t = 0.5 nm with the edges rounded by semicircular profiles and characterized by a dielectric function $1 + 4\pi i\sigma/(\omega t)$, where $\sigma(\omega)$ is the surface conductivity and ω is the light frequency. This value of t is reasonably well converged with respect to the $t \to 0$ limit (see SI), thus relieving us from the necessity of further discussing the effect of finite thickness of the graphene layer in the optical response of the structures under consideration (*cf.* the atomic-plane spacing in graphite, ~0.33 nm). The Drude model provides an instructive approximation to the conductivity and its dependence on Fermi energy E_F and relaxation time τ:

$$\sigma(\omega) = \frac{e^2 E_F}{\pi\hbar^2}\frac{i}{\omega + i\tau^{-1}}$$

We use a more realistic model for the conductivity taken from the $k_{\|} \to 0$ limit of the random-phase approximation,[58] which describes interband interactions and incorporates the effect of finite temperature (300 K). We estimate τ from the measured, impurity-limited DC mobility[20,54] $\mu \approx 10000$ cm^2/(V s), which yields $\tau = \mu E_F/ev_F^2 \approx 10^{-13}$ s for E_F = 0.1 eV, where $v_F \approx 10^6$ m/s is the graphene Fermi velocity. Actually, this is a very conservative value compared to recent observations in high-quality suspended graphene[59] (μ > 100000) and graphene on boron nitride[60] (μ = 60000). However, we are ignoring the effect of optical phonons,[18] many-body interactions,[53] and deviation from a perfect Dirac-cone band structure,[61] which should all produce an increase in the width of the modes.

Acknowledgment. This work has been supported in part by the Spanish MICINN (MAT2010-14885 and Consolider Nano-Light.es) and the European Commission (FP7-ICT-2009-4-248909-LIMA and FP7-ICT-2009-4-248855-N4E). J.C. acknowledges financial support from the Carlsberg Foundation under Contract No. QUANTONICS 2009-01-0167. A.M. acknowledges financial support through FPU from ME.

Supporting Information Available: A discussion on the convergence of our calculations with graphene thickness t, dispersion diagrams for several individual ribbons from which Figure 1c is compiled, dispersion diagrams for coplanar ribbon pairs with different separations and dielectric environment, the electrostatic scaling parameter for vertically offset ribbons, and a brief study of plasmonic waveguides based upon arrays of graphene disks. This material is available free of charge *via* the Internet at http://pubs.acs.org.

REFERENCES AND NOTES

1. Ritchie, R. H. Plasma Losses by Fast Electrons in Thin Films. *Phys. Rev.* **1957**, *106*, 874–881.
2. Myroshnychenko, V.; Rodríguez-Fernández, J.; Pastoriza-Santos, I.; Funston, A. M.; Novo, C.; Mulvaney, P.; Liz-Marzán, L. M.; García de Abajo, F. J. Modelling the Optical Response of Gold Nanoparticles. *Chem. Soc. Rev.* **2008**, *37*, 1792–1805.
3. Kociak, M.; Henrard, L.; Stéphan, O.; Suenaga, K.; Colliex, C. Plasmons in Layered Nanospheres and Nanotubes Investigated by Spatially Resolved Electron Energy-Loss Spectroscopy. *Phys. Rev. B* **2000**, *61*, 13936–13944.
4. Ju, L.; Geng, B.; Horng, J.; Girit, C.; Martin, M.; Hao, Z.; Bechtel, H. A.; Liang, X.; Zettl, A.; Shen, Y. R.; *et al.* Graphene Plasmonics for Tunable Terahertz Metamaterials. *Nat. Nanotechnol.* **2011**, *6*, 630–634.
5. Jakab, A.; Rosman, C.; Khalavka, Y.; Becker, J.; Trügler, A.; Hohenester, U.; Sönnichsen, C. Highly Sensitive Plasmonic Silver Nanorods. *ACS Nano* **2011**, *5*, 6880–6885.
6. Rodríguez-Lorenzo, L.; Álvarez-Puebla, R. A.; Pastoriza-Santos, I.; Mazzucco, S.; Stéphan, O.; Kociak, M.; Liz-Marzán, L. M.; García de Abajo, F. J. Zeptomol Detection Through Controlled Ultrasensitive Surface-Enhanced Raman Scattering. *J. Am. Chem. Soc.* **2009**, *131*, 4616–4618.
7. Duan, H.; Hu, H.; Kumar, K.; Shen, Z.; Yang, J. K. W. Direct and Reliable Patterning of Plasmonic Nanostructures with Sub-10-nm Gaps. *ACS Nano* **2011**, *5*, 7593–7600.
8. Yang, X.; Ishikawa, A.; Yin, X.; Zhang, X. Hybrid Photonic-Plasmonic Crystal Nanocavities. *ACS Nano* **2011**, *5*, 2831–2838.
9. King, N. S.; Li, Y.; Ayala-Orozco, C.; Brannan, T.; Nordlander, P.; Halas, N. J. Angle- and Spectral-Dependent Light Scattering from Plasmonic Nanocups. *ACS Nano* **2011**, *5*, 7254–7262.
10. Zhu, X.; Zhang, J.; Xu, J.; Li, H.; Wu, X.; Liao, Z.; Zhao, Q.; Yu, D. Dispersion Control in Plasmonic Open Nanocavities. *ACS Nano* **2011**, *5*, 6546–6552.
11. Nordlander, P.; Oubre, C.; Prodan, E.; Li, K.; Stockman, M. I. Plasmon Hybridizaton in Nanoparticle Dimers. *Nano Lett.* **2004**, *4*, 899–903.
12. Koh, A. L.; Bao, K.; Khan, I.; Smith, W. E.; Kothleitner, G.; Nordlander, P.; Maier, S. A.; McComb, D. W. Electron Energy-Loss Spectroscopy (EELS) of Surface Plasmons in Single Silver Nanoparticles and Dimers: Influence of Beam Damage and Mapping of Dark Modes. *ACS Nano* **2009**, *3*, 3015–3022.
13. O'Neal, D. P.; Hirsch, L. R.; Halas, N. J.; Payne, J. D.; West, J. L. Photo-Thermal Tumor Ablation in Mice Using Near Infrared-Absorbing Nanoparticles. *Cancer Lett.* **2004**, *209*, 171–176.
14. Luo, Y. L.; Shiao, Y. S.; Huang, Y. F. Release of Photoactivatable Drugs from Plasmonic Nanoparticles for Targeted Cancer Therapy. *ACS Nano* **2011**, *5*, 7796–7804.
15. Wunsch, B.; Stauber, T.; Sols, F.; Guinea, F. Dynamical Polarization of Graphene at Finite Doping. *New J. Phys.* **2006**, *8*, 318.
16. Hwang, E. H.; Das Sarma, S. Dielectric Function, Screening, and Plasmons in Two-Dimensional Graphene. *Phys. Rev. B* **2007**, *75*, 205418.
17. Hill, A.; Mikhailov, S. A.; Ziegler, K. Dielectric Function and Plasmons in Graphene. *Europhys. Lett.* **2009**, *87*, 27005.

18. Jablan, M.; Buljan, H.; Soljačić, M. Plasmonics in Graphene at Infrared Frequencies. *Phys. Rev. B* **2009**, *80*, 245435.
19. Mak, K. F.; Sfeir, M. Y.; Wu, Y.; Lui, C. H.; Misewich, J. A.; Heinz, T. F. Measurement of the Optical Conductivity of Graphene. *Phys. Rev. Lett.* **2008**, *101*, 196405.
20. Novoselov, K. S.; Geim, A. K.; Morozov, S. V.; Jiang, D.; Zhang, Y.; Dubonos, S. V.; Grigorieva, I. V.; Firsov, A. A. Electric Field Effect in Atomically Thin Carbon Films. *Science* **2004**, *306*, 666–669.
21. Zhang, Y.; Tan, Y. W.; Stormer, H. L.; Kim, P. Experimental Observation of the Quantum Hall Effect and Berry's Phase in Graphene. *Nature* **2005**, *438*, 201–204.
22. Berger, C.; Song, Z.; Li, X.; Wu, X.; Brown, N.; Naud, C.; Mayou, D.; Li, T.; Hass, J.; Marchenkov, A. N.; *et al*. Electronic Confinement and Coherence in Patterned Epitaxial Graphene. *Science* **2006**, *312*, 1191–1196.
23. Geim, A. K.; Novoselov, K. S. The Rise of Graphene. *Nat. Mater.* **2007**, *6*, 183–191.
24. Nair, R. R.; Blake, P.; Grigorenko, A. N.; Novoselov, K. S.; Booth, T. J.; Stauber, T.; Peres, N. M. R.; Geim, A. K. Fine Structure Constant Defines Visual Transparency of Graphene. *Science* **2008**, *320*, 1308.
25. Castro Neto, A. H.; Guinea, F.; Peres, N. M. R.; Novoselov, K. S.; Geim, A. K. The Electronic Properties of Graphene. *Rev. Mod. Phys.* **2009**, *81*, 109–162.
26. Geim, A. K. Graphene: Status and Prospects. *Science* **2009**, *324*, 1530–1534.
27. Bonaccorso, F.; Sun, Z.; Hasan, T.; Ferrari, A. C. Graphene Photonics and Optoelectronics. *Nat. Photon* **2010**, *4*, 611–622.
28. Schedin, F.; Lidorikis, E.; Lombardo, A.; Kravets, V. G.; Geim, A. K.; Grigorenko, A. N.; Novoselov, K. S.; Ferrari, A. C. Surface-Enhanced Raman Spectroscopy of Graphene. *ACS Nano* **2010**, *4*, 5617–5626.
29. Wallace, P. R. The Band Theory of Graphite. *Phys. Rev.* **1947**, *71*, 622–634.
30. Lee, E. J. H.; Balasubramanian, K.; Weitz, R. T.; Burghard, M.; Kern, K. Contact and Edge Effects in Graphene Devices. *Nat. Nanotechnol.* **2008**, *3*, 486–490.
31. Xia, F. N.; Mueller, T.; Lin, Y. M.; Valdes-Garcia, A.; Avouris, P. Ultrafast Graphene Photodetector. *Nat. Nanotechnol.* **2009**, *4*, 839–843.
32. Mueller, T.; Xia, F.; Freitag, M.; Tsang, J.; Avouris, P. Role of Contacts in Graphene Transistors: A Scanning Photocurrent Study. *Phys. Rev. B* **2009**, *79*, 245430.
33. Koppens, F. H. L.; Chang, D. E.; García de Abajo, F. J. Graphene Plasmonics: A Platform for Strong Light-Matter Interactions. *Nano Lett.* **2011**, *11*, 3370–3377.
34. Chen, C. F.; Park, C. H.; Boudouris, B. W.; Horng, J.; Geng, B.; Girit, C.; Zettl, A.; Crommie, M. F.; Segalman, R. A.; Louie, S. G.; *et al*. Controlling Inelastic Light Scattering Quantum Pathways in Graphene. *Nature* **2011**, *471*, 617–620.
35. Efetov, D. K.; Kim, P. Controlling Electron-Phonon Interactions in Graphene at Ultrahigh Carrier Densities. *Phys. Rev. Lett.* **2010**, *105*, 256805.
36. Novoselov, K. S.; Jiang, D.; Schedin, F.; Booth, T. J.; Khotkevich, V. V.; Morozov, S. V.; Geim, A. K. Two-Dimensional Atomic Crystals. *Proc. Natl. Acad. Sci.* **2005**, *102*, 10451–10453.
37. Bostwick, A.; Ohta, T.; Seyller, T.; Horn, K.; Rotenberg, E. Quasiparticle Dynamics in Graphene. *Nat. Photon.* **2007**, *3*, 36–40.
38. Vakil, A.; Engheta, N. Transformation Optics Using Graphene. *Science* **2011**, *332*, 1291–1294.
39. Chen, P. Y.; Alù, A. Atomically Thin Surface Cloak Using Graphene Monolayers. *ACS Nano* **2011**, *5*, 5855–5863.
40. Thongrattanasiri, S.; Koppens, F. H. L.; García de Abajo, F. J. Total Light Absorption in Graphene. arXiv:1106.4460v1.
41. Velizhanin, K. A.; Efimov, A. Probing Plasmons in Graphene by Resonance Energy Transfer. *Phys. Rev. B* **2011**, *84*, 085401.
42. Gómez-Santos, G.; Stauber T. Fluorescence Quenching in Graphene: A Fundamental Ruler and Evidence for Transverse Plasmons. arXiv:1108.1160v1.
43. Nikitin, A. Y.; Guinea, F.; García-Vidal, F. J.; Martn-Moreno, L. Fields Radiated by a Nanoemitter in a Graphene Sheet. *Phys. Rev. B* **2011**, *84*, 195446.
44. Papasimakis, N.; Luo, Z.; Shen, Z. X.; De Angelis, F.; Di Fabrizio, E.; Nikolaenko, A. E.; Zheludev, N. I. Graphene in a Photonic Metamaterial. *Opt. Express* **2010**, *18*, 8353–8359.
45. Thongrattanasiri, S.; Manjavacas, A.; García de Abajo, F. J. Unpublished work.
46. Nikitin, A. Y.; Guinea, F.; García-Vidal, F. J.; Martn-Moreno, L. Edge and Waveguide Terahertz Surface Plasmon Modes in Graphene Microribbons. *Phys. Rev. B* **2011**, *84*, 161407(R).
47. Manjavacas, A.; García de Abajo, F. J. Robust Plasmon Waveguides in Strongly Interacting Nanowire Arrays. *Nano Lett.* **2009**, *9*, 1285–1289.
48. Romero, I.; Aizpurua, J.; Bryant, G. W.; García de Abajo, F. J. Plasmons in Nearly Touching Metallic Nanoparticles: Singular Response in the Limit of Touching Dimers. *Opt. Express* **2006**, *14*, 9988–9999.
49. Berini, P. Plasmon–Polariton Waves Guided by Thin Lossy Metal Films of Finite Width: Bound Modes of Symmetric Structures. *Phys. Rev. B* **2000**, *61*, 10484–10503.
50. Berini, P. Plasmon–Polariton Waves Guided by Thin Lossy Metal Films of Finite Width: Bound Modes of Asymmetric Structures. *Phys. Rev. B* **2001**, *63*, 125417.
51. Han, M. Y.; Özyilmaz, B.; Zhang, Y.; Kim, P. Energy Band-Gap Engineering of Graphene Nanoribbons. *Phys. Rev. Lett.* **2007**, *98*, 206805.
52. Beams, R.; Cancado, L. G.; Novotny, L. Low Temperature Raman Study of the Electron Coherence Length Near Graphene Edges. *Nano Lett.* **2011**, *11*, 1177–1181.
53. Polini, M.; Asgari, R.; Borghi, G.; Barlas, Y.; Pereg-Barnea, T.; MacDonald, A. H. Plasmons and the Spectral Function of Graphene. *Phys. Rev. B* **2008**, *77*, 081411(R).
54. Novoselov, K. S.; Geim, A. K.; Morozov, S. V.; Jiang, D.; Katsnelson, M. I.; Grigorieva, I. V.; Dubonos, S. V.; Firsov, A. A. Two-Dimensional Gas of Massless Dirac Fermions in Graphene. *Nature* **2005**, *438*, 197–200.
55. Oulton, R. F.; Sorger, V. J.; Zentgraf, T.; Ma, R. M.; Gladden, C.; Dai, L.; Bartal, G.; Zhang, X. Plasmon Lasers at Deep Subwavelength Scale. *Nature* **2009**, *461*, 629–632.
56. García de Abajo, F. J.; Kociak, M. Probing the Photonic Local Density of States with Electron Energy Loss Spectroscopy. *Phys. Rev. Lett.* **2008**, *100*, 106804.
57. García de Abajo, F. J.; Howie, A. Retarded Field Calculation of Electron Energy Loss in Inhomogeneous Dielectrics. *Phys. Rev. B* **2002**, *65*, 115418.
58. Falkovsky, L. A.; Varlamov, A. A. Space–Time Dispersion of Graphene Conductivity. *Eur. Phys. J. B* **2007**, *56*, 281.
59. Bolotin, K. I.; Sikes, K. J.; Jiang, Z.; Klima, M.; Fudenberg, G.; Hone, J.; Kim, P.; Stormer, H. L. Ultrahigh Electron Mobility in Suspended Graphene. *Solid State Commun.* **2008**, *146*, 351–355.
60. Dean, C. R.; Young, A. F.; Meric, I.; Lee, C.; Wang, L.; Sorgenfrei, S.; Watanabe, K.; Taniguchi, T.; Kim, P.; Shepard, K. L.; *et al*. Boron Nitride Substrates for High-Quality Graphene Electronics. *Nat. Nanotechnol.* **2010**, *82*, 722–726.
61. Bostwick, A.; Speck, F.; Seyller, T.; Horn, K.; Polini, M.; Asgari, R.; MacDonald, A. H.; Rotenberg, E. Observation of Plastrons in Quasi-freestanding Doped Graphene. *Science* **2010**, *328*, 999–1002.

Supporting Information for "Graphene Plasmon Waveguiding and Hybridization in Individual and Paired Ribbons"

Johan Christensen,[1] Alejandro Manjavacas,[1] Sukosin Thongrattanasiri,[1]
Frank H. L. Koppens,[2] and F. Javier García de Abajo[1,*]

[1] *IQFR - CSIC, Serrano 119, 28006 Madrid, Spain*
[2] *ICFO-Institut de Ciencies Fotoniques, Mediterranean Technology Park, 08860 Castelldefels (Barcelona), Spain*

(Dated: December 1, 2011)

I. CONVERGENCE OF CALCULATED SPECTRA WITH THE WIDTH OF THE GRAPHENE LAYER

We present in Fig. 1 absorption spectra calculated for graphene ribbons using the BEM with two different values of the graphene thickness t (see Materials and Methods section in the main paper). These are in turn compared with a new discrete surface-dipole approximation method (DSDA), in which the graphene is represented by a discrete array of in-plane surface-dipole elements [2], the polarizability of which is determined to match the conductivity of homogenous graphene in an extended layer. These calculations are well converged with respect to the number of boundary elements in BEM and with the number of surface dipoles in DSDA. In practice, DSDA corresponds to an effective thickness $t = 0$. We obtain excellent agreement between DSDA and BEM for $t = 0.33\,\text{nm}$ and $t = 0.5\,\text{nm}$ in the widest ribbon under consideration ($W = 100\,\text{nm}$). However, the agreement gets increasingly worse as W decreases. This is a result of the fact that the t/W ratio increases for fixed t and decreasing W, so that eventually for $W = 25\,\text{nm}$ the values of t used are no longer in the $t/W \to 0$ limit. Even so, the main effect of finite thickness for the smallest width under consideration in the main paper ($W = 25\,\text{nm}$) is a small shift relative to the $t = 0$ plasmon energy obtained from DSDA, thus justifying the use of $t = 0.5\,\text{nm}$ throughout this work as a reasonable compromise between the degree of plasmon-energy convergence and the numerical effort required to represent such small thickness.

II. DISPERSION DIAGRAMS OF INDIVIDUAL RIBBONS FOR DIFFERENT WIDTHS AND FERMI ENERGIES

We show in Fig. 2 dispersion diagrams similar to the one depicted in Fig. 1a of the main paper, but now with different values of the ribbon width and the graphene Fermi energy. The ribbon is self-standing in all cases. The

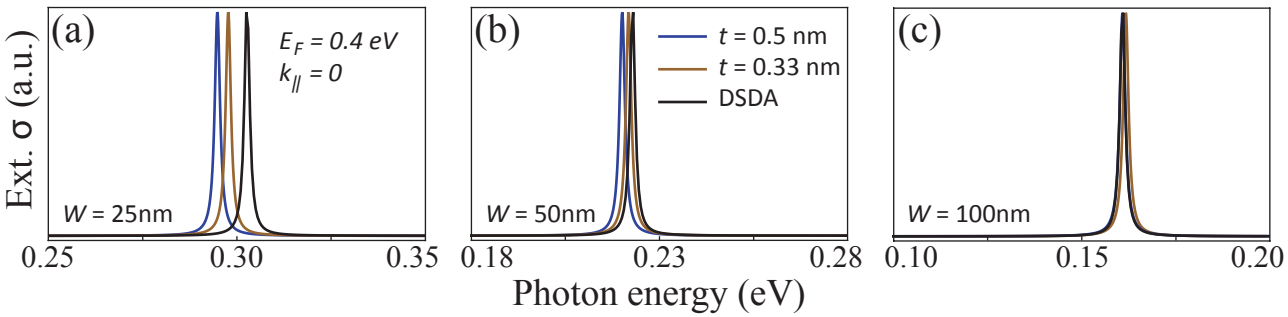

FIG. 1: Convergence of the calculated optical response with the graphene-layer thickness. **(a-c)** Absorption spectra for graphene ribbons of different widths W (see labels) computed for normally incident light ($k_{\|} = 0$) with the graphene doped up to a Fermi energy $E_F = 0.4\,\text{eV}$. Three different calculations are compared for each width: boundary element method (BEM) with two values of the graphene thickness ($t = 0.33\,\text{nm}$ and $t = 0.5\,\text{nm}$), and a DSDA method corresponding to $t = 0$ (see text for more details).

*Electronic address: J.G.deAbajo@csic.es

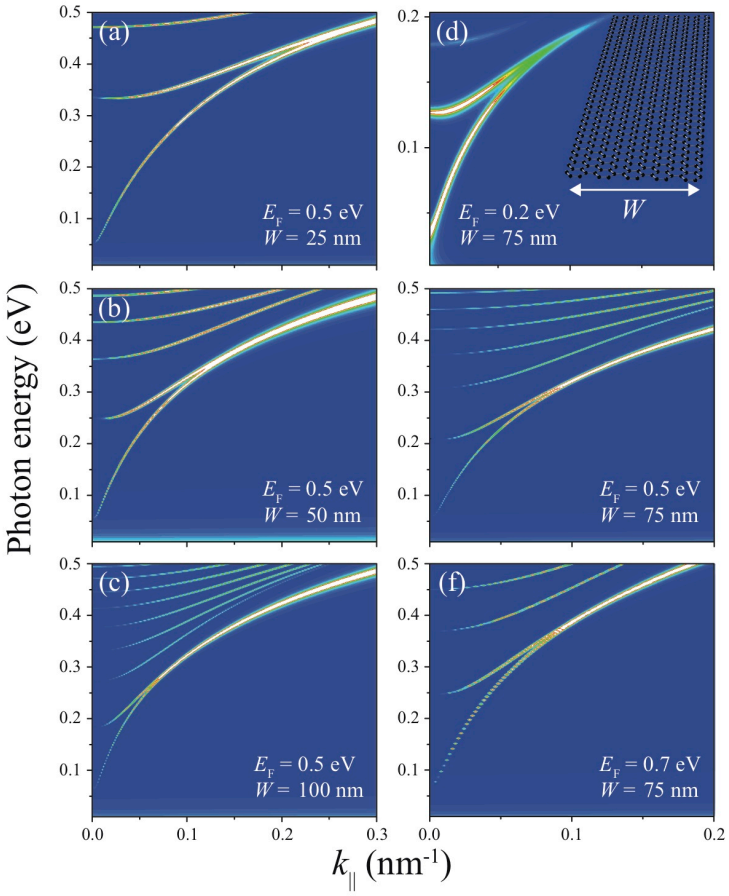

FIG. 2: **(a-d)** Dispersion diagrams of the individual self-standing ribbons considered in Fig. 1c of the main paper. The width W and Fermi energy E_F are indicated by labels in each case.

plasmon modes predicted by these diagrams are compiled in a single plot of the main paper (Fig. 1c) using the electrostatic scaling law that we discuss there.

III. DISPERSION DIAGRAMS FOR CO-PLANAR RIBBON PAIRS WITH DIFFERENT SEPARATION AND DIELECTRIC ENVIRONMENT

We show in Fig. 3 dispersion diagrams for ribbon pairs with different separations ($d = 5\,$nm and $40\,$nm in parts (a) and (b)) and dielectric environment (sitting on a silica-air interface in (a) and (b) and in a homogeneous silica environment in (d)). Mode splitting is clearly shown to decrease with separation (cf. Fig. 3a and b, and also see Fig. 3c). In a homogeneous environment (Fig. 3c), the modes are shifted towards lower energy compared to the dielectric interface. This is consistent with the electrostatic scaling law discussed in the main text.

IV. ELECTROSTATIC SCALING PARAMETER FOR VERTICALLY OFFSET RIBBONS

We show in Fig. 4 the electrostatic scaling parameter $\eta = \chi \mathrm{Im}\{\sigma(\omega_p)\}/\omega_p W$ obtained from Fig. 4c of the main paper for vertically aligned nanoribbons as a function of their separation. The original figure is calculated for ribbons embedded in silica, and therefore, we have used $\chi = 1/\epsilon_s$ with $\epsilon_s = 2.1$ in the above formula in order to compensate for the effect of the dielectric. Obviously, η depends on both the ratio d/W and the product $k_{||}W$, although we only present a limited range of values here, which can be applied to ribbons of different width W. As expected, the $d/W \gg 1$ limit yields the same result as we present in Fig. 1c of the main paper for the three lowest-energy modes of individual ribbons with $k_{||}W = 2.5$.

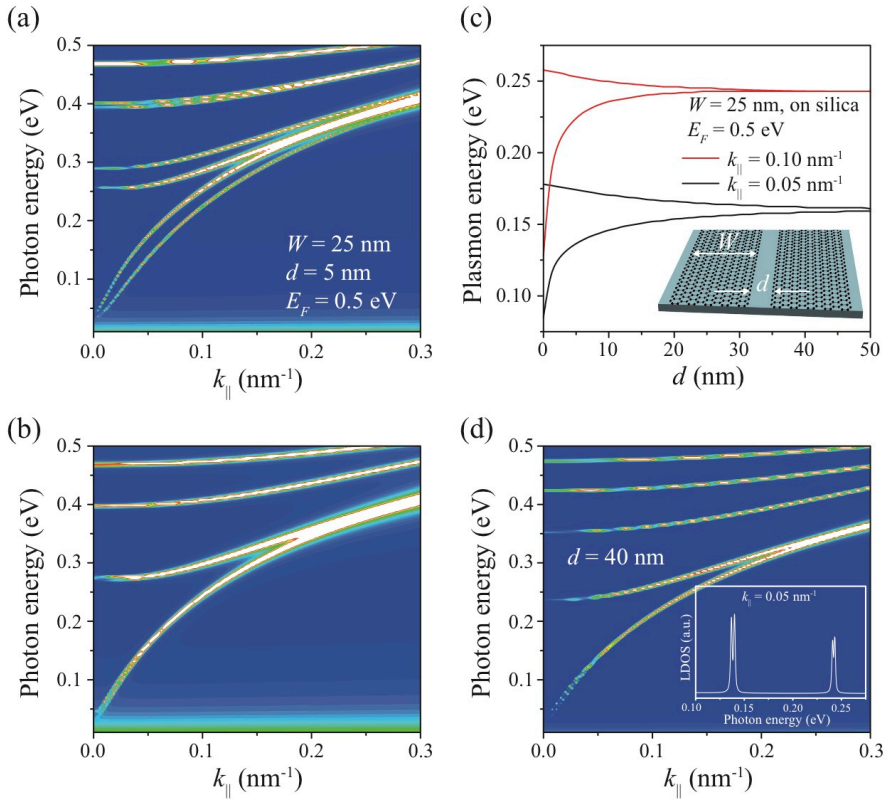

FIG. 3: **(a,b)** Dispersion diagrams for pairs of co-planar aligned ribbons of width $W = 25\,\text{nm}$ and Fermi energy $E_F = 0.5\,\text{eV}$ laying on a silica-air interface and separated a distance $d = 5\,\text{nm}$ in (a) and $d = 40\,\text{nm}$ in (b). **(c)** Plasmon energy as a function of distance d for the two lowest-energy modes in (a) and (b), and for two different values of the parallel wave vector $k_{\|}$, as indicated by labels. **(d)** Same as (b) with the ribbon pair fully embedded in a symmetric silica environment. The insets of (b) and (d) represent the spectral dependence of the LDOS at $k_{\|} = 0.05\,\text{nm}^{-1}$.

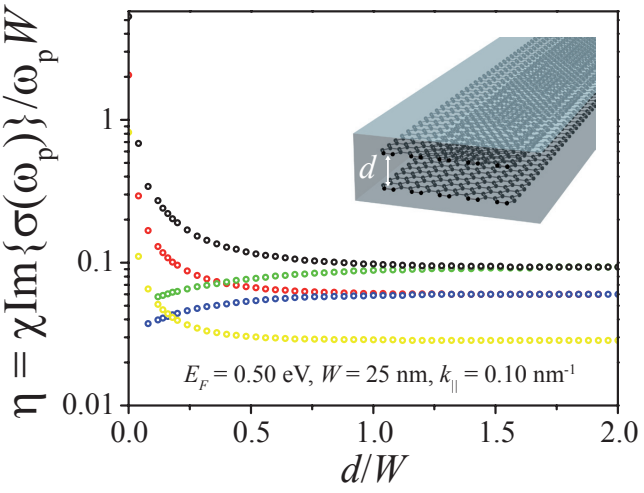

FIG. 4: Electrostatic scaling parameter extracted from the plasmon modes presented in Fig. 4c of the main paper for vertically aligned nanoribbons as a function of normalized ribbon separation. The color code is the same as in the noted figure.

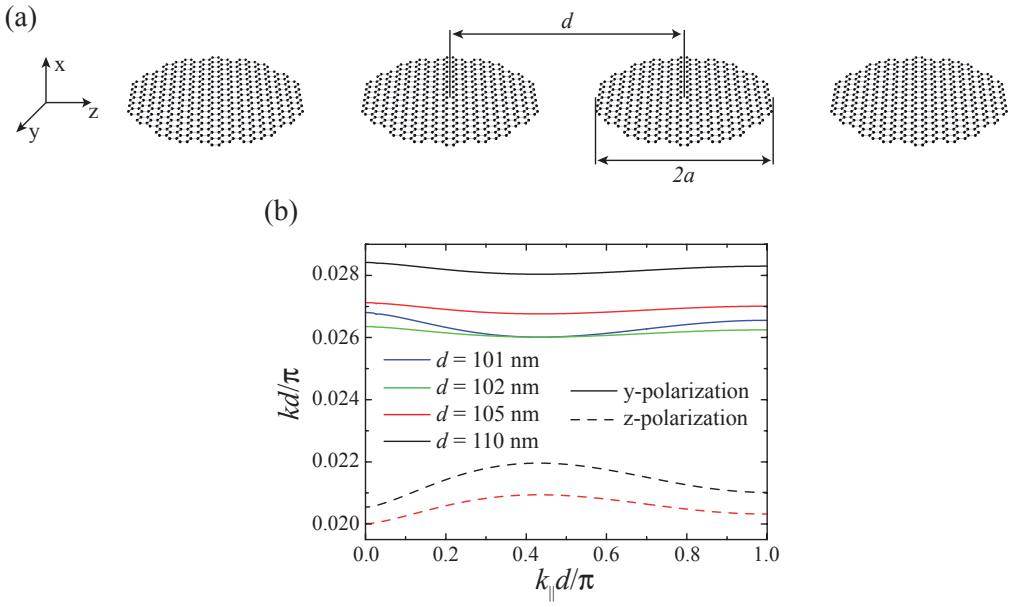

FIG. 5: Plasmonic waveguides based upon arrays of graphene disks. **(a)** Schematic view of the geometry under consideration, formed by a linear periodic array of graphene disks of radius a and period d. **(b)** Plasmon dispersion diagram for different values of d and fixed $a = 50\,\mathrm{nm}$. The conductivity of graphene is described as explained in the main paper, with the Fermi energy taken as $E_F = 0.4\mathrm{eV}$.

V. PLASMONIC WAVEGUIDES BASED UPON ARRAYS OF GRAPHENE DISKS

Doped graphene disks support localized in-plane dipole plasmons [1], and their optical response near one of these excitations is characterized by the polarizability [2]

$$\alpha(\omega) = \frac{3c^3\kappa_r}{2\omega_p^2}\frac{1}{\omega_p^2 - \omega^2 - i\kappa\omega^3/\omega_p^2},$$

where ω is the light frequency, ω_p is the plasmon frequency, κ is the plasmon decay rate, and κ_r is the partial radiative contribution to κ. The extinction cross section obtained from this analytical expression (i.e., $\sigma = 4\pi(\omega/c)\mathrm{Im}\{\alpha\}$) actually provides an excellent fit to rigorous electromagnetic solutions of Maxwell's equations for this geometry [2].

In this section we analyze the guiding properties of linear arrays of graphene disks, in which the guiding mechanism involves plasmon hopping between neighboring disks. For a mode propagating along a linear periodic array of period d (Fig. 5a), the polarization of each disk is the response to the fields produced by the rest of the disks, in addition to any possible external field. The dipole in disk j is thus determined by the self-consistent coupled-dipoles equation

$$\mathbf{p}_j = \alpha\left(\mathbf{E}_j^{\mathrm{ext}} + \sum_{j'\neq j}\mathcal{G}_{j-j'}\mathbf{p}_{j'}\right), \tag{1}$$

where $\mathbf{E}_j^{\mathrm{ext}}$ is the external field acting at the position of particle j, and $\mathcal{G}_{j-j'}$ is the dipole-dipole interaction tensor that describes the field produced on j by a dipole placed at j', a distance $R = |j-j'|d$ apart. More precisely [3],

$$\mathcal{G}_{j-j'} = \frac{e^{ikR}}{R^3}\left(k^2R^2 + ikR - 1\right)$$

when the dipoles are oriented perpendicular to the array (transversal polarization), and

$$\mathcal{G}_{j-j'} = 2\frac{e^{ikR}}{R^3}\left(ikR - 1\right)$$

for dipoles aligned with the array direction (longitudinal polarization). Here, $k = \omega/c$ is the light wave vector. For an infinite array, it is convenient to work in the space of Fourier transform, characteirzed by the parallel wave vector $k_\parallel$, and in which the transformed diples become $\tilde{\mathbf{p}}_{k_\parallel} = \sum_j \mathbf{p}_j e^{ik_\parallel jd}$. This allows us to directly write the solution of Eq. (1) as

$$\mathbf{p}_j = \frac{d}{2\pi} \int_{-\pi/d}^{\pi/d} \frac{dk_\parallel}{\alpha^{-1} - G_{k_\parallel}} \tilde{\mathbf{E}}^{\text{ext}}_{k_\parallel} e^{-ik_\parallel jd},$$

where $G_{k_\parallel} = \sum_{j\neq 0} \mathcal{G}_j e^{ik_\parallel jd}$. This expression predicts the existence of guided modes subject to the condition $\alpha^{-1} - G_{k_\parallel} = 0$. Incidentally, the lattice sum for transversal polarization is poorly convergence and we use the methods described in [4] to obtain fast and accurate results.

So far, this theory is only valid in the dipolar approximation, in which we assume the array period d to be large compared to the disk radius a (i.e., $d \gg a$). However, we can easily extend it to include higher-order terms beyond the dipole in the nearest-neighbor interaction, which results in much higher degree of accuracy allowing us to even study nearly touching disks. This is simply achieved by replacing the dipolar nearest-neighbor interaction by a coupling strength derived from rigorous numerical simulations of the extinction cross section of a graphene disk dimer. The dipolar approximation is maintained for the interactions between second-nearest neighbors and beyond.

Figure 5b shows dispersion diagrams of guided modes supported by arrays of graphene disks with different values of the period d. The dispersion relations are given both for polarization along the array (dashed curves, longitudinal modes) and perpendicular to the array (solid curves, transversal modes). Incidentally, polarization normal to the disks is forbidden for strictly 2D disks. The longitudinal modes show up at lower energies due to stronger attractive interaction between nearest neighbors. At small separations ($d - 2a = 1$ and 2 nm), these longitudinal modes lie outside the energy range under consideration, although the validity of our theory, based upon a local description of the graphene conductivity, is questionable in that limit. In general, the dispersion curves are rather flat, thus describing nearly localized modes, with only a small degree of hopping.

[1] F. H. L. Koppens, D. E. Chang, and F. J. García de Abajo, Nano Lett. **11**, 3370 (2011).
[2] S. Thongrattanasiri and F. J. García de Abajo, arXiv:1106.4460v1.
[3] J. D. Jackson, *Classical Electrodynamics* (Wiley, New York, 1999).
[4] F. J. García de Abajo, Phys. Rev. E **61**, 5743 (2000).